

## Pipe Network Model for Scaling of Dynamic Interfaces in Porous Media

Chi-Hang Lam<sup>1</sup> and Viktor K. Horváth<sup>2</sup>

<sup>1</sup>*Department of Applied Physics, Hong Kong Polytechnic University, Hung Hom, Hong Kong, China*

<sup>2</sup>*Department of Physics, University of Pittsburgh, Pittsburgh, Pennsylvania 15260  
and Department of Biological Physics, Eötvös University, 1117 Budapest, Hungary*

(Received 1 February 2000)

We present a numerical study on the dynamics of imbibition fronts in porous media using a pipe network model. This model quantitatively reproduces the anomalous scaling behavior found in imbibition experiments [Phys. Rev. E **52**, 5166 (1995)]. Using simple scaling arguments, we derive a new identity among the scaling exponents in agreement with the experimental results.

PACS numbers: 47.55.Mh, 05.40.-a, 05.70.Ln, 68.35.Fx

Self-affine interfaces are found in a variety of phenomena such as two-phase flow in porous media, thin film deposition, flame fronts, etc. [1]. In particular, scaling properties of imbibition fronts have been the focus in many experimental studies [2–4]. Static scaling behavior has been suggested to be described by a directed depinning percolation model [2,5–7]. To explain dynamic properties, one needs to go beyond local models and properly deal with the effects of long-range coupling through pressure. Much progress has been obtained using theoretical approaches including consideration of capillary waves [8], a Flory-type scaling argument [9], and very recently a phase-field model [10]. These studies contributed to our better understanding of the scaling behavior of imbibition. However, exponents provided in general do *not* compare satisfactorily with the experimental values. In fact, of the four exponents determined experimentally by Horváth and Stanley [3] with good precision, *none* have previously been explained analytically or numerically, and no existing exponent identity applies. In this work, we successfully reproduce all these exponents using a pipe network model once the relevant model parameters are properly fine-tuned. A new exponent identity among these exponents is also presented. In addition, we have found an empirical relation between the spatial and temporal correlations.

Horváth and Stanley studied imbibition fronts climbing up in vertical filter paper sheets which move continuously downward into a water container at constant speed  $v$  [3]. The interface height at horizontal coordinate  $x$  and time  $t$  is denoted by  $h(x, t)$ . The average height  $\bar{h}$  and width  $w$  were demonstrated to scale as

$$v \sim \bar{h}^{-\Omega}, \quad w \sim v^{-\kappa}. \quad (1)$$

The temporal height-height correlation function  $C(t) = \langle [h(x, t' + t) - h(x, t')]^2 \rangle^{1/2}$  [11] was shown to follow a scaling form,

$$C(t) = v^{-\kappa} f(tv^{(\theta + \kappa)/\beta}), \quad (2)$$

where  $f(u) \sim u^\beta$  for small  $u$ , and it converges to a constant for large  $u$ . The exponents were found to be

$$\Omega = 1.594, \quad \kappa = 0.48, \quad \theta_t = 0.37, \quad \beta = 0.56. \quad (3)$$

The first exponent has particularly strong implications because Darcy's law, which is well established for many porous media [12], implies  $\Omega = 1$ . The same result was also found in numerous numerical studies [10,13,14]. Physically, the anomalous value  $\Omega = 1.594$  suggests that as the interface height increases its propagation speed becomes slower than simple considerations of capillary pressure and viscous drag would suggest. This cannot be explained by gravity, evaporation, deformation of wetted paper [10], or inertial effects [12] since they involve intrinsic length or time scales and can introduce only transients or cutoffs to Darcy's prediction.

Our network model consists of cylindrical pipes connecting volumeless nodes on a two-dimensional square lattice with periodic boundary conditions in the horizontal direction. According to Poiseuille's law [12], the flow rate in a pipe of radius  $r$  is  $Q = \pi r^4 \Delta p / 8 \mu d$  where  $\Delta p$  is the pressure difference between two points separated by  $d$ . The fluid viscosity is denoted by  $\mu$ . The pressure at the water level in the tank is maintained at the atmospheric value. The capillary pressure is  $2\gamma \cos\phi / r$  in each partially filled pipe where  $\gamma$  and  $\phi$  are the surface tension and the contact angle, respectively. Gravity is neglected. This is because in Ref. [3], scalings were reported only for  $\bar{h}$  smaller than 65% of the maximum value limited by gravity at  $v = 0$  [15]. We have checked numerically that gravity is negligible in this range, even though it can lead abruptly to the breakdown of Eq. (1) at larger  $\bar{h}$  and finally to the pinning transition. We calculate the pressure at every wetted node above the water level of the tank by solving Kirchhoff's equations using a locally adaptive overrelaxation method. The propagation of the interface during the associated adaptive time step is hence computed. For computational convenience, possible deviation from Poiseuille's law at the junction of the pipes is neglected as usual [13] and menisci cannot retreat after reaching a node. Since in a real situation air can escape from either side of the sheet, trapping of air is irrelevant and its flow is not simulated.

The pipe model at this point is similar to those in previous studies [12–14] most of which focused on flow inside porous rocks. Tenuous percolation-type wetting patterns are obtained. To simulate more compact patterns observed in paper, we therefore implement a new wettability rule to impose a strong effective surface tension in our network. Now, water can enter an empty pipe from a wetted node only if the neighborhood is sufficiently wet. Specifically, of the eight most nearby nodes (the four nearest and the four next nearest neighbors) forming a loop around the node under consideration, there must exist a connected subset of five which are already wet. This is the most stringent criterion for the wettability of pipes connected to a wetted node without halting the imbibition entirely or involving consideration of further neighbors. It leads to a very strong effective surface tension. Different and more detailed wettability rules were discussed in Ref. [14]. In addition, fluid pathways in randomly arranged fibers have complicated geometry and there is an abundance of narrow bottlenecks and large pores. We therefore propose another important characteristic of our network, namely, large spatial fluctuations in local properties. Its implementation will be discussed later.

The model was first tested in the presence of small fluctuations. Adopt a unit lattice spacing and specify the fluid properties by  $\mu = \gamma \cos\phi = 1$  [16]. We assume random pipe radii in the range  $[0, 0.5]$  uniformly distributed [17]. This distribution is broader than those used by others [13,14]. Darcy's prediction  $\Omega = 1$  is readily verified.

To simulate large fluctuations expected in real paper, we simply replace a fraction  $p_w$  of pipes by wider ones with radius  $r_w$ . For sufficiently large  $p_w$  and  $r_w$ ,  $\Omega > 1$  is obtained. Both exponents  $\Omega$  and  $\kappa$  then depend non-trivially but continuously on  $p_w$  and  $r_w$ . Fortunately, we have found that nice power laws with the experimental values of  $\Omega$  and  $\kappa$  can be reproduced if we put  $p_w = 0.18$  and  $r_w = 2.0$  [17]. We will adopt these parameters in the remainder of this work [18]. Snapshots of simulations of imbibition in stationary sheets are shown in Fig. 1.

We have simulated imbibition in moving paper sheets considered in Ref. [3]. This involves continuous upward shifting of the level on the lattice which represents the contact line of the paper sheet with the water in the reservoir. The interface height  $\bar{h}$  and width  $w$  are measured after steady state has been attained and are averaged over three independent runs using lattices of width 200 and height 1000. Figures 2(a) and 2(b) plot, respectively,  $v$  and  $w$  against  $\bar{h}$ . The linearity observed in log-log plots verifies the scaling relations in Eq. (1). We get  $\Omega = 1.62 \pm 0.05$  and  $\kappa = 0.49 \pm 0.03$  close to the experimental values in Eq. (3) due to the fine-tuning of the pipe distribution mentioned above. The quoted errors represent only the uncertainties in the linear fits.

The spatial correlation  $C(l) = \langle [h(x+l, t) - h(x, t)]^2 \rangle^{1/2}$  and the temporal counterpart  $C(t)$  defined earlier are computed and plotted in Figs. 3(a) and 3(b), respectively. The initial linear regions corresponding

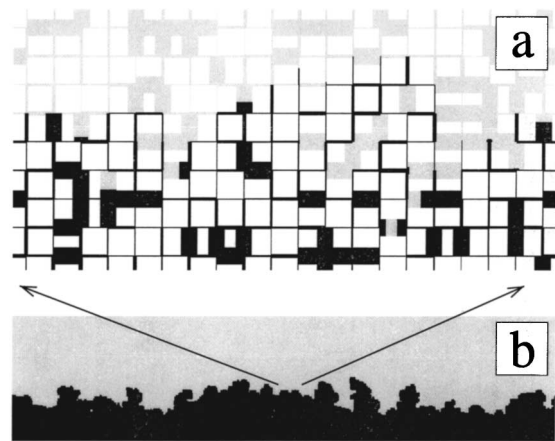


FIG. 1. (a) Snapshot of a small scale simulation showing individual pipes. Wet and dry regions are shaded in black and grey, respectively. Radii of pipes have been scaled down. (b) Snapshot of the wetted region in a larger scale simulation on a lattice of width 500. The average height is 36.8. The arrows provided are only to demonstrate the ratio of the scales of the two figures.

to  $C(l) \sim l^\alpha$  and  $C(t) \sim t^\beta$  for small  $l$  and  $t$  give  $\alpha = 0.61 \pm 0.01$  and  $\beta = 0.63 \pm 0.01$ , respectively. This value of  $\beta$  is in reasonable agreement with the experimental value 0.56. We have verified that  $C(t)$  in Fig. 3(b) follows the experimentally motivated scaling forms in Eq. (2) and we obtain  $\theta_t = 0.38 \pm 0.02$  in excellent agreement with the experimental value 0.37. Similarly, the spatial correlation follows an analogous scaling form  $C(l) = v^{-\kappa} g(lv^{(\theta_l + \kappa)/\alpha})$  where  $g(u) \sim u^\alpha$  for small  $u$  and it converges to a constant for large  $u$ . A further result is obtained by first reparametrizing  $C(t)$  by the vertical displacement  $z = vt$  of the sheet. Equation (2) then becomes  $C(z) = v^{-\kappa} f(zv^{(\theta_z + \kappa)/\beta})$ , where

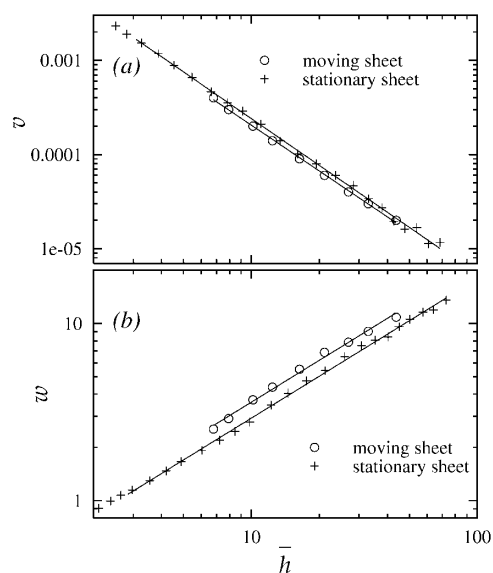


FIG. 2. Log-log plots of (a)  $v$  and (b)  $w$  against  $\bar{h}$ . In (a), the fitted lines have slopes  $-1.62$  and  $-1.65$  for the moving and stationary case, respectively. In (b), they are  $0.785$  and  $0.786$ .

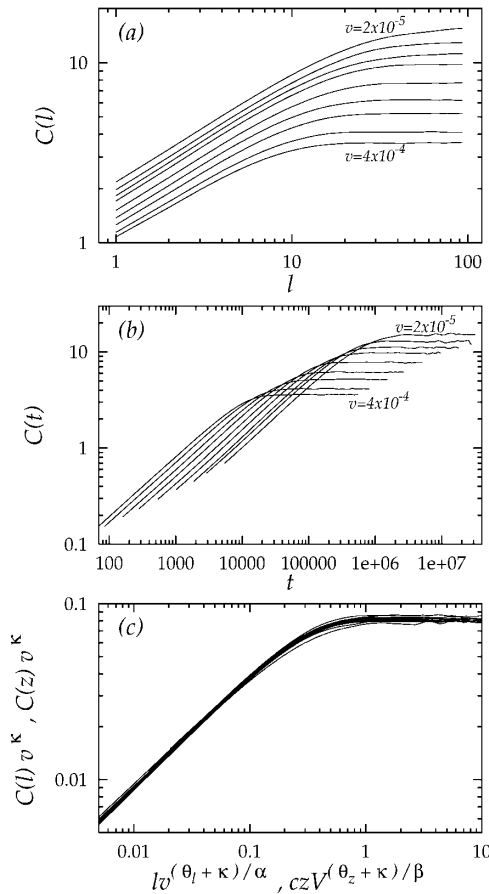


FIG. 3. Log-log plots of (a) spatial correlation, (b) temporal correlation, and (c) simultaneous data collapse of all correlation curves in both (a) and (b) for paper speed  $v$  given by  $v/10^{-5} = 2, 3, 4, 6, 9, 14, 20, 30$ , and 40.

$\theta_z = \theta_l - \beta$ . We note that both  $C(l)$  and  $C(z)$  can be collapsed individually using a common set of exponents  $\alpha = \beta = 0.62$  and  $\theta_l = \theta_z = -0.24$ . Furthermore, they can all be collapsed together as shown in Fig. 3(c) verifying the empirical identities

$$\alpha = \beta, \quad \theta_l = \theta_z, \quad f(cu) = g(u), \quad (4)$$

where  $c = 1.6$ .

Next, we simulate imbibition in stationary paper sheets. The interface height  $\bar{h}$  and width  $w$  averaged over seven lattices of width 1000 are found to scale as

$$\bar{h} \sim t^\epsilon, \quad w \sim t^{\beta_w}, \quad (5)$$

where  $\epsilon = 0.374 \pm 0.005$  and  $\beta_w = 0.29 \pm 0.01$ . The interface speed  $v(t) = \bar{h}/dt$  hence computed from direct numerical differentiation on our data is plotted as a function of  $\bar{h}$  in Fig. 2(a). The width  $w$  is also plotted against  $\bar{h}$  in Fig. 2(b). Direct comparison with the moving sheet results is possible because the paper speed  $v$  in that case is also the average interface speed in the paper frame. These plots show that the scaling relations in Eq. (1) apply to stationary sheets with the same exponents as well. Therefore, we can derive Eq. (1) from Eq. (5) and vice versa. In the derivation, one obtains

$$\epsilon = \frac{1}{\Omega + 1}, \quad \beta_w = \frac{\Omega \kappa}{\Omega + 1}, \quad (6)$$

which describe our exponents accurately.

For a stationary sheet,  $w$  at a given  $\bar{h}$  is only about 80% of the corresponding value for a moving sheet as observed from Fig. 2(b). The roughness has therefore not yet fully developed for the given height  $\bar{h}$ . In contrast, for the less noisy case the roughness has saturated completely and can be determined solely from  $\bar{h}$  [10]. More importantly, our result indicates that the roughness gets neither closer to nor farther from saturation as  $\bar{h}$  increases since  $w$  is always 80% of the saturated value. This constancy of the degree of saturation implies that the system has a unique dynamic time scale dictating both the growth of the roughness and the steady state dynamics of a roughened interface. The time it takes to develop a width  $w$  is  $w^{1/\beta_w}$  from Eq. (5). It is thus proportional to the relaxation time extracted from the temporal correlation function  $v^{-(\theta_l + \kappa)/\beta} \sim w^{(\theta_l + \kappa)/(\beta \kappa)}$  from Eqs. (1) and (2). Therefore,  $1/\beta_w = (\theta_l + \kappa)/(\beta \kappa)$ . Applying Eq. (6), we have

$$\beta = \Omega(\theta_l + \kappa)/(\Omega + 1). \quad (7)$$

This identity is particularly important because all values have been measured experimentally in Ref. [3]. Inserting the experimental values into the right-hand side of Eq. (7), we get  $\beta = 0.52$  in reasonable agreement with the experimental value 0.56. Using our numerical estimates instead, we get  $\beta = 0.54$  which is a little smaller than the numerically found value 0.61. In the latter case we relate the discrepancy to errors in the numerical determination of  $\beta$ . This may be due to lattice discretization effects which become more important at  $C(t) \lesssim 1$ . The spatial counterpart  $\alpha$  should hence suffer a similar problem. Furthermore, noticeably different values of  $\alpha$  and  $\beta$  are obtained if correlations of higher moments are used [10].

The good agreement between our numerical results and the experimental ones strongly supports the fact that our model has captured the essential physics in the imbibition process. However, some further points are yet to be considered. First, despite the nice power-law fits and data collapses of the relevant quantities observed, existence of extraordinarily slow crossover effects masking different asymptotic scalings should be cautioned. Second, our model reproduces the experimental results after fine-tuning of the radius distribution. We have also found a few other completely different distributions which also lead to similar exponents upon fine-tuning [18]. The exponents nevertheless are *not* robust with respect to changes in the details of the models. Using distributions other than the fine-tuned ones, the exponents are in general different and sometimes scalings may not even hold [18]. We expect that there is a yet unknown selection mechanism so that models generating the experimental exponents are preferred. This is currently under active investigation. However, one cannot determine *a priori* a correct realistic pipe distribution. This is

because all pipe networks are simplified models of fluid pathways which are indeed very different from those of paper. Realistic simulations, for example, using the lattice-Boltzmann method with sophisticated boundary conditions in three dimensions [19] unfortunately covers only microscopic regions and thus cannot be applied to study the macroscopic scalings.

Finally, local models of imbibition have been classified into isotropic and anisotropic universality classes exemplified, respectively, by the random field Ising model (RFIM) and the directed percolation depinning (DPD) model [6]. The anisotropy in the DPD model is due to a solid-on-solid condition. In contrast, for our model both the wettability rule and the flow dynamics treat the horizontal and vertical directions equivalently. Concerning the local symmetry, it is more closely related to the isotropic class. It was found that  $\alpha = 1$  and  $\beta_w = 3/4$  for the isotropic class [6], while  $\epsilon = \alpha = \beta_w \simeq 0.633$  for the anisotropic one [5] at criticality. This is to be compared with  $\epsilon \simeq 0.374$ ,  $\alpha \simeq 0.61$ , and  $\beta_w \simeq 0.29$  for our model. It is easy to see that the much larger values of  $\epsilon$  and  $\beta_w$  for DPD and also  $\beta_w$  for RFIM are due to the locality of the interactions. We believe that the agreement of  $\alpha$  between DPD and our model is just a coincidence. The morphologies of the surfaces are indeed visually quite different. Previous works on nonlocal models including pipe networks and the phase-field model [10,13,14] are in a weak fluctuations regime and are all consistent only with Darcy's law. Our pipe network with strong fluctuations is the only model exhibiting distinctly different scalings in good agreement with the experimental ones in Ref. [3]. We therefore suggest that it belongs to a new universality class.

In conclusion, we have simulated imbibition in paper using a pipe network model and reproduced all scaling behaviors observed experimentally in Ref. [3]. We obtain

$$\Omega = 1.62, \quad \kappa = 0.49, \quad \theta_t = 0.38, \quad \beta = 0.63, \quad (8)$$

which is to be compared with Eq. (3). The model displays rich behavior, and can be tuned to reproduce the experimentally determined values of  $\Omega$  and  $\kappa$ . Then  $\beta$  and  $\theta_t$  turn out, respectively, in reasonable and excellent agreement with the experimental values. Assuming a single time scale in the dynamics, we have presented a new exponent identity [Eq. (7)] which is justified by the experimental values. Two other exponent identities in Eq. (6) relating the moving and stationary paper cases are deduced and verified numerically. Further identities in Eq. (4) for exponents and scaling functions are suggested empirically based on a data collapse between the spatial and temporal correlations.

We have benefited from helpful communications with L. M. Sander, M. Rost, M. Dubè, T. Ala-Nissila, and F. G. Shin who are gratefully acknowledged. C. H. L. is supported by Project No. B-Q075 from the Research

Grants Council of Hong Kong SAR. V. K. H. is supported by the Hungarian Science Foundation Grant No. OTKA-F17310 and NATO Grant No. DGE-9804461.

- 
- [1] A.-L. Barabási and H. E. Stanley, *Fractal Concepts in Surface Growth* (Cambridge University Press, Cambridge, England, 1995).
  - [2] S. V. Buldyrev *et al.*, Phys. Rev. A **45**, R8313 (1992).
  - [3] V. K. Horváth and H. E. Stanley, Phys. Rev. E **52**, 5166 (1995).
  - [4] L. A. N. Amaral *et al.*, Phys. Rev. Lett. **72**, 641 (1994); F. Family, K. C. B. Chan, and J. G. Amar, *Surface Disorder, Roughening and Phase Transitions* (Nova Science, Commack, NY, 1992), p. 205; T. H. Kwon, A. E. Hopkins, and S. E. O'Donnell, Phys. Rev. E **54**, 685 (1996); O. Zik *et al.*, Europhys. Lett. **38**, 509 (1997).
  - [5] L.-H. Tang and H. Leschhorn, Phys. Rev. A **45**, R8309 (1992).
  - [6] L. A. N. Amaral, A.-L. Barabási, and H. E. Stanley, Phys. Rev. Lett. **73**, 62 (1994); L.-H. Tang, M. Kardar, and D. Dhar, Phys. Rev. Lett. **74**, 920 (1995).
  - [7] R. Albert, A.-L. Barabási, N. Carle, and A. Dougherty, Phys. Rev. Lett. **81**, 2926 (1998).
  - [8] E. G. Flekkøy and D. H. Rothman, Phys. Rev. Lett. **75**, 260 (1995).
  - [9] V. Ganesan and H. Brenner, Phys. Rev. Lett. **81**, 578 (1998).
  - [10] M. Dubè *et al.*, Phys. Rev. Lett. **83**, 1628 (1999).
  - [11] More precisely,  $C(t) = \langle [\tilde{h}(x, t') - \tilde{h}(x, t' + t)]^2 \rangle^{1/2}$  in Ref. [3], where  $\tilde{h}(x, t) = h(x, t) - \bar{h}(t)$ . The two definitions are equivalent for wide paper sheets or pipe networks since the spatially averaged height  $\bar{h}(t) \equiv \bar{h}$  is then time independent at steady state. For narrower networks used in our simulations, our definition suffers smaller finite size effects and can better approximate the results in Ref. [3] where wide sheets were used.
  - [12] M. Sahimi, *Flow and Transport in Porous Media and Fractured Rock* (VCH, Weinham, 1995).
  - [13] E. Aker, K. J. Måløy, and A. Hansen, Phys. Rev. E **58**, 2217 (1998).
  - [14] M. J. Blunt and H. Scher, Phys. Rev. E **52**, 6387 (1995).
  - [15] V. K. Horváth (unpublished).
  - [16] From dimensional analysis, this amount to transforming length, time, and fluid density with the respective multiplicative factors  $a_0^{-1}$ ,  $a_0^{-1} \mu_0^{-1} \gamma_0 \cos \phi$ , and  $a_0 \mu_0^{-2} \gamma_0 \cos \phi$ , respectively. Here,  $a_0$ ,  $\mu_0$ , and  $\gamma_0$  are the lattice spacing, viscosity, and surface tension, respectively, in physical units.
  - [17] According to the dynamics we have defined, enlarging or reducing the radii of *all* pipes by an overall multiplicative factor is only equivalent to a transformation of units similar to that in Ref. [16] and is of no physical significance. Possible physical overlapping of pipes is hence irrelevant and is naturally neglected in our dynamical equations.
  - [18] Results on other pipe distributions will be presented elsewhere.
  - [19] A. Koponen *et al.*, Phys. Rev. Lett. **80**, 716 (1998).